The use of 4-methylbenzenesulfonate ionic liquid derivatives as environmentally friendly corrosion inhibitors for mild steel in hydrochloric acid

T. Nesane[1], S.S. Mnyakeni-Moleele[1], and L.C. Murulana[1]

Affiliation:

[1] Department of Chemistry, School of Mathematical and Natural Sciences, University of Venda, Private Bag X5050, Thohoyandou 0950, South Africa.

Correspondence to:
L.C. Murulana

Email:
Lutendo.murulana@univen.ac.za

ORCID
T. Nesane
https://orchid.org/0000-0003-2066-1124
S.S. Mnyakeni-Moleele
https://orchid.org/0000-0002-7124-9124
L.C. Murulana
https://orchid.org/0000-0001-5889-3794

Synopsis

The effectiveness of two synthesized ionic liquids, 1-(benzyloxy)-1-oxopropan-2-aminium 4-methylbenzenesulfonate (1-BOPAMS) and 4-(benzyloxy)-4-oxobutan-1-aminium 4-methylbenzene-sulfonate (4-BOBAMS), were evaluated for mild steel corrosion inhibition in 1.0 M hydro-chloric acid solution, using electrochemical impedance spectroscopy (EIS), potentiodynamic polarization (PDP), and gravimetric techniques. Organic moieties responsible for the adsorption process on mild steel surface were investigated using Fourier transform infrared spectroscopy (FTIR). Gravimetric analysis revealed that the inhibition efficiency of 1-BOPAMS and 4-BOBAMS increased with concentration, with maximum inhibition values of 90.32% and 97.91%, respectively, at the highest concentration of the inhibitors. Gibbs free energy ($\Delta G°$ads) values indicated a strong interaction between the mild steel surface and the molecules of the ionic liquids, and that the adsorption process was spontaneous. These values also show that the inhibitive nature of ionic liquids against mild steel corrosion is caused by a mixed-type of adsorption film formed on the steel surface. The Langmuir adsorption isotherm was used to describe the adsorption of ionic liquid molecules onto the mild steel surface. Polarization curves showed that 1-BOPAMS and 4-BOBAMS have a similar effect on both the anodic and cathodic half-reactions, indicating that they prevent the dissolution of mild steel through both physical and chemical process. Nyquist plots were defined by incomplete semicircle capacitive loops, showing that the charge transfer mechanism controls the corrosion of mild steel in acidic solution.

Keywords
corrosion inhibition, ionic liquids, mild steel, adsorption isotherm.

Introduction

An inhibitor that is both effective and environmentally friendly, as well as inexpensive and which produces the desired effect at low concentrations, is preferable for use against metal corrosion. Some studies have been devoted to the subject of corrosion inhibitors (Musa, Jalgham, and Mohamad 2012; Nataraja, Venkatesha, and Tandon, 2012). Corrosion inhibitors protect against corrosion by forming protective films on the metal surface, diminishing any possible contact of the metal surface with the corrosive environment. For inhibitors to be able to protect the metal from corrosion, they must first reach the metal surface and electrochemically react with, or be adsorbed onto, the metal surface (Cisse *et al.*, 2011; Raja *et al.*, 2016). As such, they must have centres or functional groups in their molecules with a high electron density from which they can donate electrons to the metal surface, resulting in the coordination of the inhibitor to the metal surface (Chaubey, Quraishi, and Ebenso, 2015; Raja *et al.*, 2016).

Mild steel (MS) has many applications in industries, but readily undergoes rusting (oxidation) when exposed to corrosive environments (Kim, Kim, and Moon, 2011). Ionic liquids (ILs) are preferred as corrosion inhibitors due to their chemical structure, which contains both organic and inorganic functional groups that act as centres of adsorption onto metal surfaces (Lozano *et al.*, 2014). Zheng *et al.* (2014) studied the use of ILs as corrosion inhibitors for MS in sulphuric acid, and found that they acted as an effective mixed-type inhibitor with a predominantly cathodic nature. Although the use of some ILs as corrosion inhibitors has been reported, owing to their physicochemical

The use of 4-methylbenzenesulfonate ionic liquid derivatives

properties further studies of other ILs are warranted due to the potential for discovering excellent inhibitors for metals in different corrosive environments. As such, the prime aim of the present study was to synthesize, and investigate the effectiveness of, two ILs, 4-(benzyloxy)-4-oxobutan-1-aminium 4-methylbenzenesulfonate (4-BOBAMS) and 1-(benzyloxy)-1-oxopropan-2-aminium 4-methylbenzenesulfonate (1-BOPAMS), as potential inhibitors for MS corrosion in 1.0 M HCl.

Experimental procedure

Materials

MS with a composition of Mn 0.37 wt% , Ni 0.039 wt%, P 0.02 wt%, S 0.03 wt%, C 0.21 wt%, Fe 99.32 wt%, and Mo 0.01 wt% was used in all experimental procedures. The MS coupons had a length of 3 cm and a breadth of 2 cm and contained a small hole 2 mm in diameter for hanging on a glass rod.

Preparation of solutions

1.0 M HCl solution was prepared by diluting analytical grade (32%) HCl with double-distilled water. Stock solutions of 10.0×10^{-3} M of the two corrosion inhibitors were prepared by weighing appropriate amounts of the synthesized compounds in a 1000 ml volumetric flask. From each stock solution of the inhibitor, a series of solutions of different concentrations was prepared. All the experiments were carried out at a 1:1 ratio of 1.0 M HCl and the inhibitor of interest.

Synthesis of 1-BOPAMS and 4-BOBAMS

The two IL inhibitors were synthesized by suspending alanine (6.2124 g, 69.7395 mmol) and γ-amino butanoic acid (7.0164 g, 68.0411 mmol) respectively, with 10 ml benzoyl alcohol (10.4 g, 96.1716 mmol) in a mixture of toluene (PhMe) (200 ml) and p-toluenesulfonic acid monohydrate (PTSA) (14.5821 g, 84.6812 mmol). The mixture was refluxed for 10 hours with azeotropic removal of water. The products obtained were precipitated by the addition of diethyl ether (Et$_2$O) (100 ml), filtered, dissolved in CH$_3$OH (60 ml), and further precipitated by the addition of Et$_2$O (100 ml). Figure 1 shows the reaction scheme followed for the synthesis of the two compounds. The products were obtained as white crystals, filtered, and dried. 1-BOPAMS (C17H21NO5S, mol. wt. 351.42), yield:

22.3816 g, 91% and 4-BOBAMS (C$_{18}$H$_{23}$NO$_5$S, mol. wt. 365.44), yield: 23.0146 g, 93%. Spectral analysis was carried out to confirm the two ionic liquids.

Weight loss measurements

The initial mass of the MS coupons was noted before they were immersed completely in 100 ml of 1.0 M HCl in the absence and presence of different concentrations of 1-BOPAMS and 4-BOBAMS and at various temperatures ranging from 30–60°C for 8 hours. This was done in a thermostatic water bath to maintain the temperature during the immersion period. After 8 hours, the specimens were removed, washed with double-distilled water, and dried. After drying, the final weights of the specimens were noted using a PW-254 Adam analytical balance at four decimal places.

Electrochemical techniques

Electrochemical measurements were carried out using a Metrohm Autolab potentiostat/galvanostat (PGSTAT302N). The corrosion cell consisted of the MS as the working electrode, a platinum counter-electrode, and a saturated calomel electrode (SCE) as a reference electrode. The MS was left to corrode freely for 30 minutes to attain a stable value of E_{corr} in an open circuit potential (OCP) *versus* SCE before any tests was started. The EIS analysis was carried out at a frequency range of 100 kHz to 0.00001 kHz under OCP conditions with an amplitude 5 mV peak to actual peak, using an AC signal at E_{corr}. The PDP curves were recorded at a potential range of –250 to +250 mV (*vs* SCE) and a scan rate of 1 mV.s^{-1}. The semicircle of the Nyquist plots was fitted to obtain the impedance parameters using Equation [1]:

$$\% \, IE_{EIS} = \left(1 - \frac{R^{\circ}{}_{ct}}{R_{ct}} \right) \times 100 \qquad [1]$$

where $\%IE_{EIS}$ is the percentage inhibition efficiency from the electrochemical impedance spectroscopy data, $R^{\circ}{}_{ct}$ is the charge transfer resistance in the absence of the inhibitor, and R_{ct} is the charge transfer resistance in the presence of the inhibitor.

Tafel curves (anodic and cathodic) obtained from the PDP measurements were extrapolated to obtain the electrochemical parameters. Equation [2] was used to calculate inhibition efficiencies (%IEPDP).
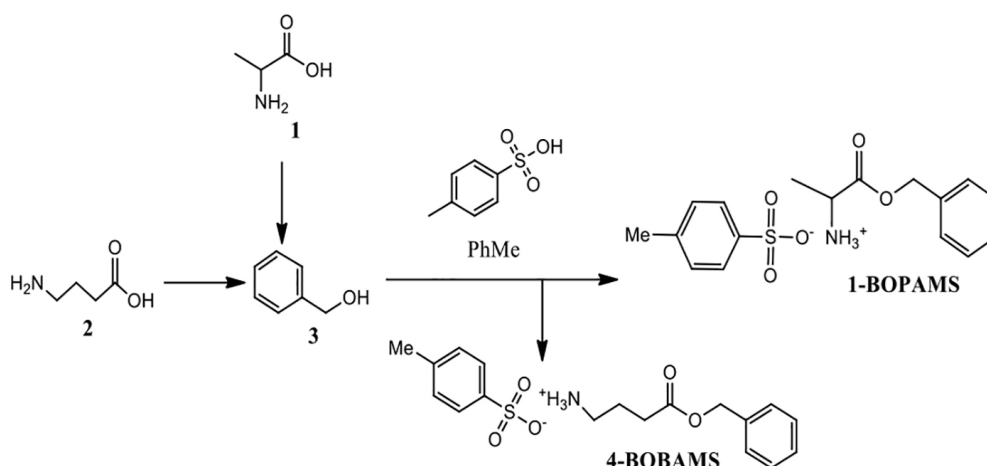

Figure 1—Schematic of the synthesis of 1-BOPAMS and 4-BOBAM. (1) Alanine, (2) γ-amino butanoic acid, (3) benzoyl alcohol

$$\%IE_{PDP} = \left(\frac{i^{\circ}corr - i^{i}corr}{i^{\circ}corr} \right) \times 100 \qquad [2]$$

where, $\%IE_{PDP}$ is the percentage inhibition efficiency from the potentiodynamic polarization data, i°_{corr} is the corrosion current density in the absence of an inhibitor, and i^{i}_{corr} is the corrosion current density in the presence of an inhibitor.

Results and discussion

Characterization of 4-BOBAMS and 1-BOPAMS

Figure 2 shows the ¹H-NMR and ¹³C-NMR spectra of 1-BOPAMS. The ¹H-NMR spectra were characterized by a broad singlet peak accounting for three protons at 8.36 ppm. The spectra also had two doublets which account for two protons each at 7.50 ppm and 7.13 ppm. The aromatic region (this is the region of the NMR
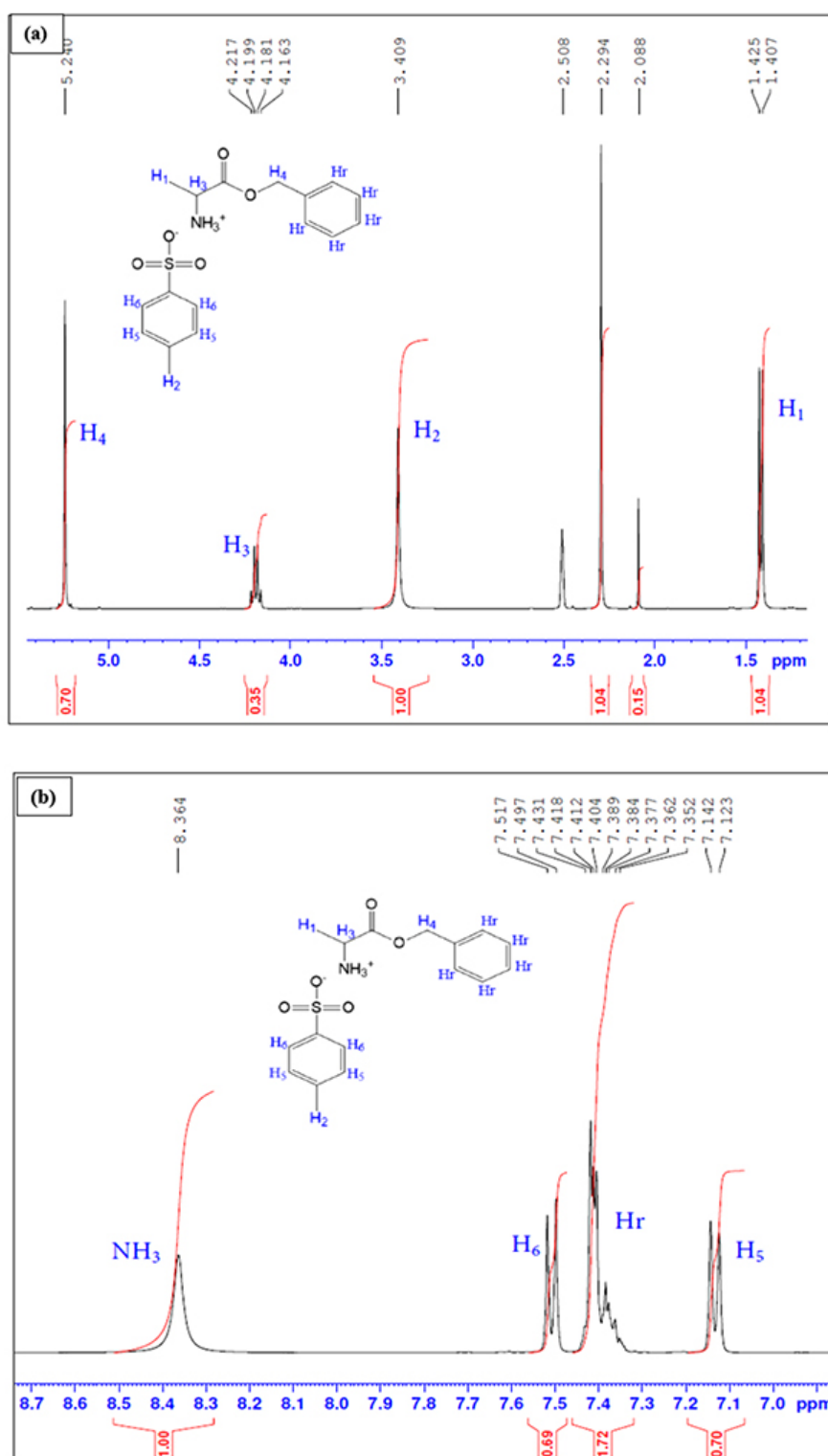

Figure 2—¹H-NMR and ¹³C-NMR spectra of 1-BOPAMS, where (a) and (b) represent the ¹H-NMR spectrum and (c) represents the ¹³C-NMR spectrum
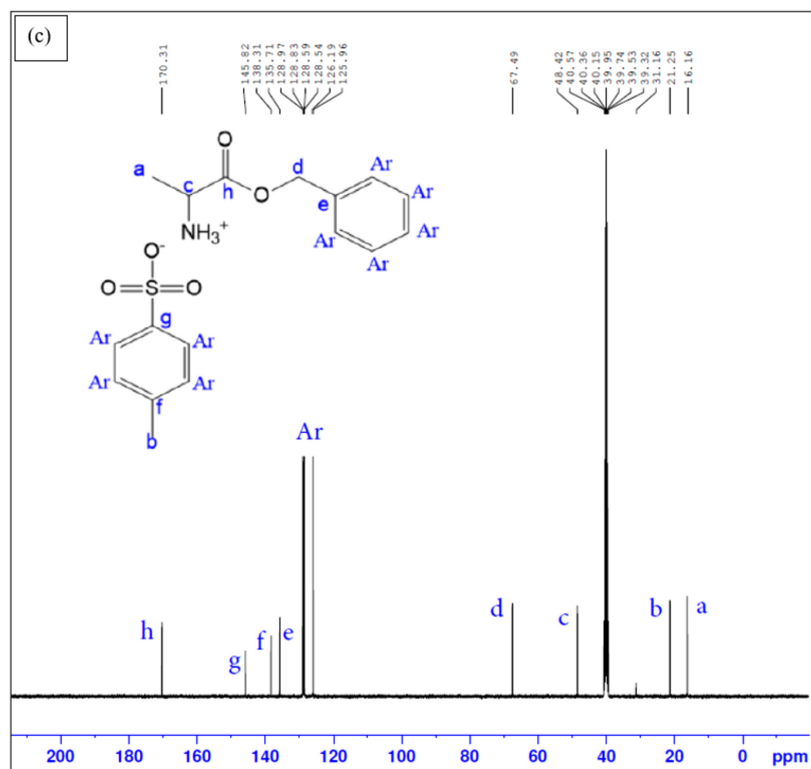
Figure 2—¹H-NMR and ¹³C-NMR spectra of 1-BOPAMS, where (a) and (b) represent the ¹H-NMR spectrum and (c) represents the ¹³C-NMR spectrum *(continued)*

spectrum where aromatic protons, which are protons attached to the benzene rings of the ILs, appear) was characterized by a multiplet accounting for five protons at about 7.4 ppm. The heteroatomic and aliphatic regions of 1-BOPAMS were characterized by a doublet accounting for three protons at 1.41 ppm, a singlet accounting for three protons at 3.41 ppm, and another singlet accounting for two protons at 5.34 ppm. The presence of a quintet accounted for single protons at around 4.18 ppm. The ¹³C-NMR spectra represent the accurate number of carbon atoms present in the chemical structures of the compounds used at the appropriate chemical shift values. Two methyl carbon peaks were observed at around 16.16 ppm ($H_3C(3)$Aln) and 21.25 ppm ($H_3C(3)$PTSA). A methine carbon peak was observed at approximately 31.16 ppm (HC(2)Aln) and a methylene carbon peak at around 67.49 ppm (H_2CBn). The aromatic protons of the benzene rings were found at around 125–128 ppm (CAr), and four quintenary peaks at about 135, 138, 145, and 170 ppm (CO_2Bn). 4-BOBAMS was characterized in a similar way as 1-BOPAMS and both the 1H-NMR spectra and ¹³C-NMR are comparable to those of 1-BOPAMS.

Electrochemical impedance spectroscopy (EIS)

An electrode equivalent circuit can be fitted to interpret experimental data collected from EIS, where the individual elements of the circuit correspond to the electrochemical properties of the tested system (Macdonald, 1992); in this case, 1.0 M HCl in the absence and presence of 4-BOBAMS and 1-BOPAMS corrosion inhibitors. Figures 3a and 3b shows the blank fitted Nyquist plot and the three-element equivalent circuit model used to measure the impedance of the two ILs. The circuit included the solution resistance (R_s) represented by (R_1), charge transfer resistance (R_{ct}), represented by (R_2), and (Q_1) represents the constant phase element (CPE) (Y_o).

Figure 4 shows that the Nyquist plots obtained consisted of capacitive loops in the absence and presence of different concentrations of the inhibitors at 30°C. The plots are represented by incomplete semicircle capacitive loops. This imperfection indicates that the charge transfer process governs the corrosion of MS in acidic solutions (Jacob and Parameswaran, 2010) and is possibly due to factors such as the frequency dispersion, distribution of surface active sites, inhomogeneity of the metal surface, grain boundaries, surface roughness, and impurities. In such cases, CPE is usually introduced in the circuit to model a complex impendence system to get a more accurate fit (Ehsani *et al.*, 2014a, 2014b). CPE is characterized by a fixed phase shift angle and its impedance is defined by Equation [3]:

$$Z_{CPE} = \frac{1}{Y_0(j\omega)^n} \qquad [3]$$

where, Z_{CPE} is the constant phase element impedance, Y_o (CPE constant) and n (CPE exponent) are parameters related to phase shift angle, ω is the angular frequency ($\omega = 2\varpi f$, where f is the AC frequency), and j is the imaginary unit (Yadav, Quraishi, and Maiti, 2012).

The significant change in the impedance response in the presence of the inhibitors can be attributed to the increase in the incomplete semicircle capacitive loop diameter with the increase in the inhibitor concentration, which specifies the increasing coverage of the MS surface. The electrochemical impedance parameters derived from Nyquist plots and the %IEEIS values are listed in Table I. The R_{ct} values are directly proportional to the corrosion inhibition efficiency and provide details on the magnitude of the electron transfer over the surface of the MS (Jacob and Parameswaran, 2010).

It can be observed from Table I that by raising the inhibitor concentration, the R_{ct} values also increased while the CPE
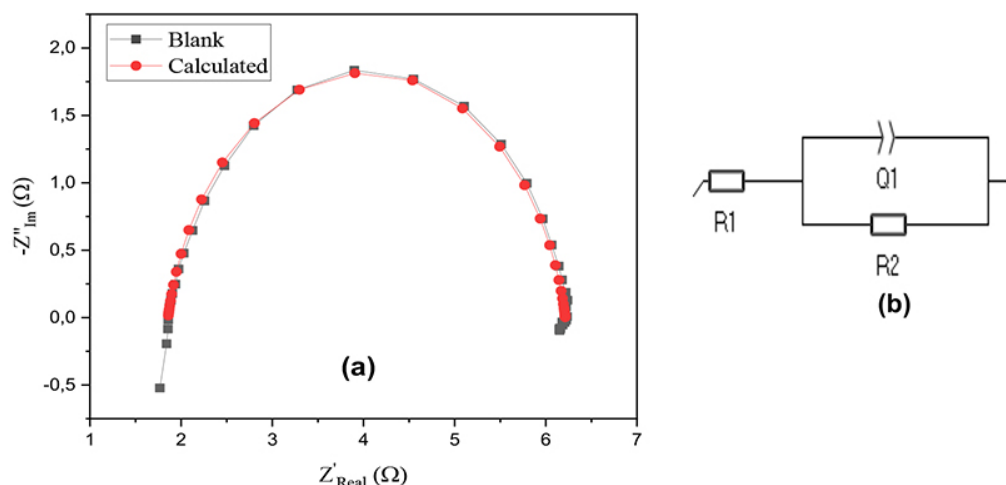
Figure 3 – Stimulated circuit fit (a) and equivalent circuit (b) used to fit the impendence data for MS corrosion in 1.0 M HCl at 30°C

Table I

Electrochemical impedance spectroscopy (EIS) parameters including the inhibitor concentration (C_{inh}), resistance of charge transfer (R_{ct}), constant phase element (Y_o), solution resistance (R_s), CPE exponent (n), and the surface coverage (θ) for MS corrosion in 1.0 M HCl in absence and presence of different concentrations of 1-BOPAMS and 4-BOBAMS at 30°C

| Inhibitor	C_{inh} (M)	R_{ct} (Ω)	Y_o (F.s$^{(a-1)}$)	R_s (Ω)	n	θ	IE_{EIS} (%)
Blank	–	4.37	0.26e-3	1.867	0.8827	–	–
	1.0 x10^{-3}	9.98	0.25e-3	2.314	0.8787	0.5627	56.27
	2.0 x10^{-3}	16.06	0.181e-3	2.665	0.8551	0.7282	72.82
	3.0 x10^{-3}3	17.75	0.26e-3	6.478	0.8729	0.7541	75.41
1-BOPAMS	4.0 x10^{-3}	24.11	0.15e-3	2.360	0.8795	0.8190	81.90
	5.0 x10^{-3}	57.50	0.14e-3	2.827	0.8958	0.9241	92.41
	1.0 x10^{-3}	17.57	0.20e-3	2.391	0.8833	0.7541	75.41
	2.0 x10^{-3}	17.75	0.26e-3	6.478	0.8729	0.7541	75.41
	3.0 x10^{-3}	19.46	0.16e-3	3.578	0.8938	0.7757	77.57
4-BOBAMS	4.0 x10^{-3}	58.05	0.22e-3	3.950	0.8352	0.9248	92.48
	5.0 x10^{-3}	94.62	0.22e-3	2.885	0.8571	0.9539	95.39
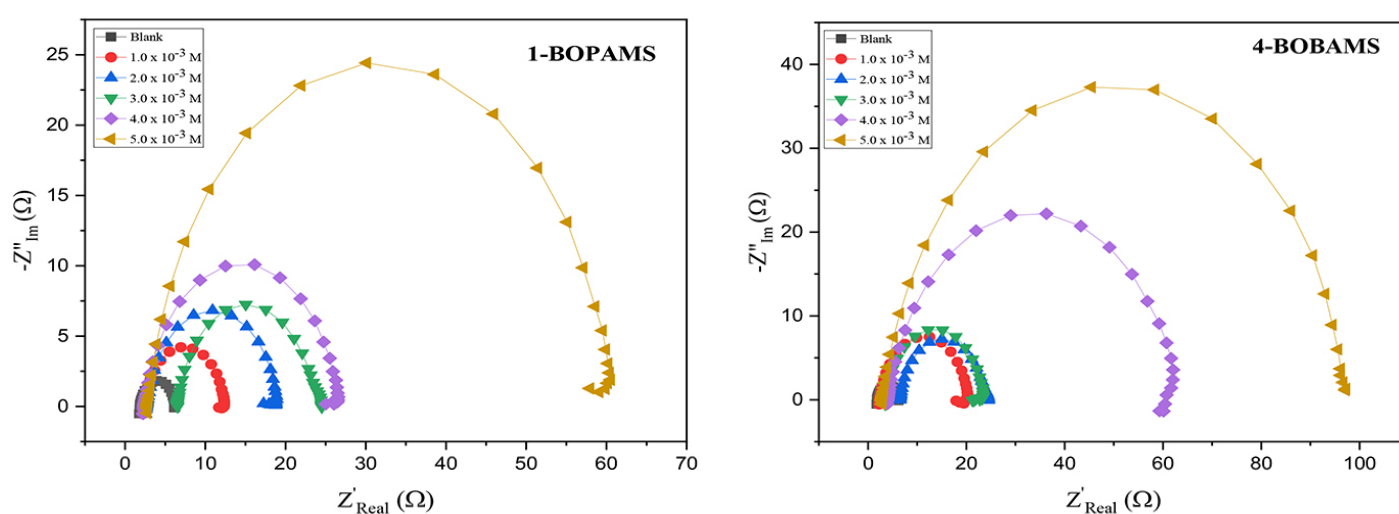
Figure 4 – Nyquist plots for MS in 1.0 M HCl in the absence and presence of different concentrations of 1-BOPAMS and 4-BOBAMS at 30°C

decreased. This is because the addition of inhibitor increased the surface coverage on the MS by the inhibitor molecules, and due to the formation of a protective film which resulted in a decrease of the electron transfer between the metal surface and the corrosive medium (Chetouani, 2002). The CPE constant for both inhibitors at all studied concentrations decreased compared to the blank. The decrease in Y_o after the addition of the inhibitors may be due to either an increase in the thickness of the double

layer (this is a layer that is formed on the surface of the metal when it is in contact with the corrosive solution in the presence of the inhibitors) or to the desorption of water molecules from MS followed by the adsorption of the inhibitor onto the metal surface. The CPE indicates a reduction in the local dielectric constant or an enhancement in the thickness of the electric double layer.

Potentiodynamic polarization (PDP)

PDP measurements were carried out to understand the role of inhibitors in biasing anodic and cathodic reactions of MS. Before running any tests, the system was allowed to reach a constant potential at an open circuit. Anodic and cathodic Tafel curves for MS corrosion in 1.0 M HCl solution were obtained in the absence and presence of various concentrations of 4-BOBAMS and 1-BOPAMS at 30°C (Figure 5). Potentiodynamic parameters such as corrosion potential (E_{corr}), corrosion current density (i_{corr}), anodic (β_a) and cathodic (β_c) Tafel slopes, and linear polarization resistance were extrapolated from these curves, and the results are shown in Table II.

The Tafel curves and Table II show that the i_{corr} decreased markedly upon introduction of the two inhibitors both in the anodic and cathodic regions, indicating that the inhibitors are adsorbed onto the MS surface and inhibit the corrosion process. An inhibitor can be classified as anodic or cathodic type if the change in the E_{corr} values is greater than ±85 mV (Mashuga *et al.*, 2015). In the present study, the magnitude of the shifted E_{corr} values in the presence of ILs compounds was towards

more negative values and the shift was less than 85 mV at all inhibitor concentrations with respect to the blank solution, which implies that these are mixed-type inhibitors that control both the cathodic and anodic reactions of the MS. Nesane, Mnyakeni-Moleele, and Murulana (2020) observed a similar trend in the shift of E_{corr} values caused by the same inhibitors against aluminium corrosion. On the other hand, the addition of different concentrations of these inhibitors in 1.0 M HCl solution altered the Tafel slopes (β_a and β_c) to approximately the same extent, supporting the concept that both the retardation of the anodic metal dissolution and cathodic hydrogen reduction were affected (Hegazy, Ahmed, and El-Tabei, 2011).

The variation of β_a and β_c in the presence of the inhibitors compared to the blank can be attributed to the change in the kinetics of hydrogen evolution as a result of the diffusion or barrier effect (Tourabi *et al.*, 2013). The cathodic polarization curves are almost parallel to each other, indicating that the hydrogen evolution reaction is under activation control (Thanapackiam *et al.*, 2016). The change in β_a values with the addition of the inhibitors suggests that the inhibition process could be attributed to the formation of an adsorption film on the metal surface, thus impeding the corrosion of MS by blocking the active sites of the metal without affecting the anodic reaction mechanism (Abdel-Rehim, Khaled, and Al-Mobarak, 2011). The addition of the ILs surfactants to the corrosive solution resulted in an increase in the R_p values, which increased to a maximum at the highest concentration of the surfactants used in
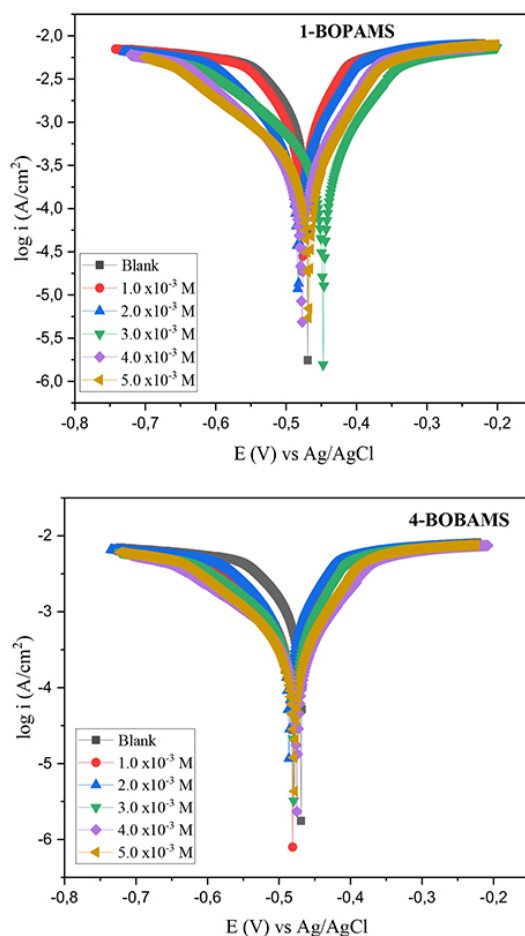

Figure 5—Tafel plots for MS in 1.0 M HCl in the absence and presence of different concentrations of 1-BOPAMS and 4-BOBAMS inhibitor compounds (shown by different colours)

Table II

Potentiodynamic polarization (PDP) parameters including the inhibitor concentration (C_{inh}), corrosion potential (E_{corr}), corrosion current density (i_{corr}) and anodic and cathodic Tafel slopes (β_a and β_c) for MS corrosion in 1.0 M HCl in both the presence and absence of different concentrations of 1-BOPAMS and 4-BOBAMS at 30°C

Inhibitor	C_{inh} (M)	E_{corr} (mV)	i_{corr} (mAcm^{-2})	β_a (mVdec^{-1})	β_c (mVdec^{-1})	R_p (10^{-1}) (Ω cm²)	IE_{PDP} (%)	IE_{WL} (%)
Blank	–	−469	0.00212	20	26	22.97	–	–
	1.0 x10^{-3}	−477	0.00067	8	10	28.33	68.55	78.63
	2.0 x10^{-3}	−483	0.00023	5	6	54.60	89.40	83.43
1-BOPAMS	3.0 x10^{-3}	−447	0.00030	9	13	79.69	86.33	84.77
	4.0 x10^{-3}	−478	0.00023	8	11	87.46	89.11	88.75
	5.0 x10^{-3}	−468	0.00017	7	10	100.34	91.92	90.32
	1.0 x10^{-3}	−481	0.00045	7	11	41.04	78.67	92.73
4-BOBAMS	2.0 x10^{-3}	−486	0.00045	6	8	33.40	78.71	94.51
	3.0 x10^{-3}	−480	0.00033	7	10	52.38	84.28	97.65
	4.0 x10^{-3}	−475	0.00026	8	12	82.16	87.75	97.70
	5.0 x10^{-3}	−478	0.00024	7	10	76.82	88.67	97.91

Table III

Weight loss measurements of MS in 1.0 M HCl containing various concentrations of 1-BOPAMS and 4-BOBAMS at different temperatures (where Cinh stands for inhibitor concentration, CR stands for corrosion rate, and IE stands for inhibition efficiency)

Inhibitor	Cinh (M)	30°C		40°C		50°C		60°C	
		CR (g.cm^{-2}.h^{-1})	IE (%)	CR (g.cm^{-2}.h^{-1})	IE (%)	CR (g.cm^{-2} h^{-1})	IE (%)	CR (g.cm^{-2}.h^{-1})	IE (%)
Blank	–	0.00717	–	0.01320	–	0.02437	–	0.04099	–
1-BOPAMS	1.0×10-3	0.00153	78.63	0.00432	67.27	0.00909	62.72	0.01797	56.17
	2.0×10-3	0.00189	83.43	0.00404	69.37	0.00860	64.73	0.01725	57.93
	3.0×10-3	0.00109	84.77	0.00399	69.80	0.00848	65.19	0.01692	58.73
	4.0×10-3	0.00081	88.75	0.00383	71.01	0.00733	69.92	0.01650	59.75
	5.0×10-3	0.00069	90.32	0.00340	74.23	0.00715	70.68	0.01569	61.73
4-BOBAMS	1.0×10-3	0.00052	92.73	0.00296	77.59	0.00990	59.38	0.01880	53.28
	2.0×10-3	0.00039	94.51	0.00283	78.54	0.00931	61.81	0.01899	54.13
	3.0×10-3	0.00017	97.65	0.00261	80.24	0.00898	63.14	0.01776	56.68
	4.0×10-3	0.00017	97.70	0.00205	84.49	0.00882	63.80	0.01686	58.88
	5.0×10-3	0.00015	97.91	0.00180	86.40	0.00833	65.81	0.01576	61.56

this study, indicating an effective inhibition by the compounds. The increase in the R_p values with the increase in inhibitor concentration implies that further polarization of MS was opposed by the formation of an adsorption film formed by the inhibitor molecules present in the solution at the metal/solution interface. The %IEPDP values obtained increased with the increased concentration of both inhibitors.

Effect of temperature and inhibitor concentration

The corrosion rate (C_R) and %IE in the absence and presence of various concentrations of 4-BOBAMS and 1-BOPAMS in 1.0 M HCl solution and at different temperatures (30–60°C) are presented in Table III. The addition of 4-BOBAMS and 1-BOPAMS markedly decreased the corrosion rate of MS and the decrease was proportional to the increase in the concentration of the inhibitors. In the uninhibited system, the weight loss was higher and decreased at a faster rate as the temperature of the solution was increased from 30°C to 60°C. The acceleration in the weight loss can be attributed to the increase in collisions between the HCl molecules and the MS surface. However, when an inhibitor was introduced into the solution, the weight loss decreased significantly; this was due to the formation of a surface film by the adsorption of the inhibitor molecules, which acted as a barrier between the aggressive HCl molecules and MS surface.

Even in the presence of the inhibitors in solution, the %IE decreased as the temperature was increased, possibly due to the

desorption of the inhibitors on the MS surface. For instance, the %IE of 1-BOPAMS at 30°C is 90.32%, decreasing to 61.73% at 60°C for the highest concentration of 5.0 ×10^{-3} M. This behaviour was observed for both inhibitors. The protective properties of the inhibitors are possibly a result of the interaction between ϖ-electrons and heteroatoms (ϖ-electrons are electrons that are involved in a ϖ-bond between two atoms (this can be in form of double or triple bonds), and heteroatoms are any atoms other than carbon or hydrogen, such as sulphur, oxygen, and nitrogen, that are in the two chemical structures of the compounds utilized in this study) with the positively charged MS surface (Mu *et al.*, 2006).

Adsorption considerations

The data obtained from the weight loss analysis was fitted to several isotherms. The Langmuir adsorption isotherm gave the best description for the synthesized compounds on MS in 1.0 M HCl solution. The Langmuir adsorption isotherm is calculated from Equation [4].

$$\frac{C_{inh}}{\theta} = \frac{1}{K_{ads}} + C_{inh} \qquad [4]$$

where C_{inh} is the concentration of the inhibitor, K_{ads} is the equilibrium constant of adsorption, and θ is the surface coverage.

The plots of C_{inh}/θ *versus* C_{inh} gave a straight line (Figure 6) with a regression coefficient (R²) around unity, confirming that the adsorption of 4-BOBAMS and 1-BOPAMS on a MS surface in 1.0 M HCl obeyed the Langmuir adsorption isotherm. From these figures, the equilibrium constant of adsorption (K_{ads}) was obtained from the slopes and enabled the calculation of the free Gibbs energy using Equation [5].

$$\Delta G°_{ads} = -RT\ln(55.5K_{ads}) \qquad [5]$$

where, the value 55.5 is the molar concentration of water in the solution, $\Delta G°_{ads}$ is the standard Gibbs free energy of adsorption, R is the universal gas constant, T is the absolute temperature (all in metric units), and K_{ads} is the equilibrium constant of adsorption.

The values of $\Delta G°_{ads}$ around –0 kJ.mol⁻¹ and lower are consistent with the electrostatic interaction between charged molecules and the charged surface of the substrate (physisorption), which is a process that involves weak Van der Waals interaction rather than chemical bonding (Musa, Jalgham, and Mohamad, 2012). Conversely, those that are around –40 kJ.mol⁻¹ and above correspond to chemical adsorption (chemisorption), which occurs through the sharing or transfer of an electron from the adsorbate molecules on the surface of MS resulting in a coordinate type of bond. The $\Delta G°_{ads}$ values (Table IV) were negative, indicating the spontaneity of the adsorption process and that there was a strong interaction between the inhibitor molecules and MS surface (Hegazy, Ahmed, and El-Tabei, 2011). The $\Delta G°_{ads}$ values that are around –20 kJ.mol⁻¹, and also those around –40 kJ.mol⁻¹, implied that mixed-type

adsorption took place, *i.e.*, a mixture of both physisorption and chemisorption.

The trends of these values elaborate on the nature of the adsorption that occurs between the MS surface and the corrosion inhibitors. Thiraviyam and Kannan (2013) found that increased $\Delta G°_{ads}$ with increased temperature indicates exothermic adsorption, whereas decreasing $\Delta G°_{ads}$ with increased temperature indicates endothermic adsorption. In the present study, the $\Delta G°_{ads}$ values increased as the temperature increased, indicating that the adsorption mechanism between the MS surface and the two inhibitors was exothermic, which signifies either chemisorption or physisorption mechanisms.

Adsorption film analysis

Figure 7 reveals that some of the functional groups observed in the pure compounds disappeared, and these functional groups can be said to be responsible for the complex formation with the MS surface, preventing the dissolution process. The FTIR spectra for the adsorption film formed show that the intensity of the peaks decreased, indicating that a coordinate bond was created through the functional groups of these peaks, with the Fe^{2+}, forming the Fe^{2+}-inhibitor complex on the surface of the MS, preventing the dissolution process. The FTIR spectra for the two pure ILs, 4-BOBAMS and 1-BOPAMS, were similar and showed an ammonium salt ($^+NH_3$) which gave a strong, broad absorption band at around 3066–3095 cm⁻¹. The intensity of these peaks decreased and shifted to about 3326 cm⁻¹. The peaks located around 630–660 cm⁻¹ represent the Fe-O stretching bond frequency, indicating the modification of the MS surface by the
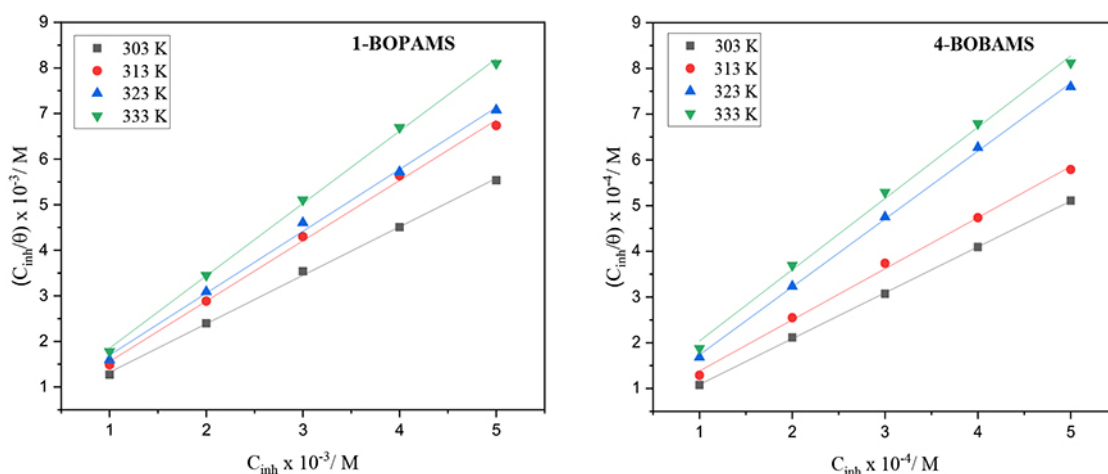

Figure 6—Langmuir adsorption isotherm plots for the adsorption of different concentrations of 1-BOPAMS and 4-BOBAMS on the surface of MS in 1.0 M HCl at different temperatures

Table IV

Thermodynamic and adsorption parameters for MS in 1.0 M HCl at various temperatures for 1-BOPAMS and 4-BOBAMS

Inhibitor	T (K)	R²	Slope	K_{ads} (L.mol⁻¹)	$\Delta G°ads$ (kJ.mol⁻¹)
1-BOPAMS	303	0.9985	1.0638	3864.29	–30.9266
	313	0.9971	1.3249	4296.82	–32.2234
	323	0.9962	1.3590	2949.16	–32.2422
	333	0.9985	1.5881	3806.91	–33.9473
4-BOBAMS	303	0.9999	1.0035	12025.01	–33.7866
	313	0.9976	1.1184	3790.46	–31.8971
	323	0.9992	1.4861	4009.78	–33.0673
	333	0.9966	1.5589	2086.51	–32.2823

The use of 4-methylbenzenesulfonate ionic liquid derivatives
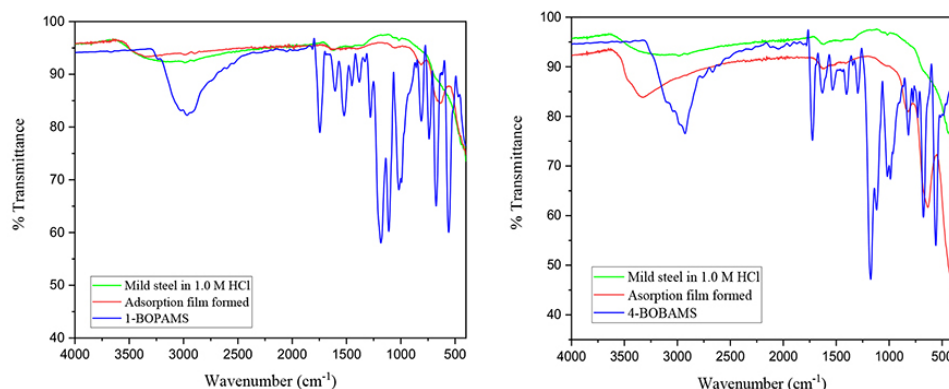

Figure 7—FTIR spectra for the pure compound and adsorption films formed on the MS in 1.0 M HCl by 1-BOPAMS and 4-BOBAMS corrosion inhibitors

formation of a Fe-inhibitor complex through the oxygen atoms present in the structures of the compounds. The peaks around 3326.22 cm^{-1} and 1614.52 cm^{-1} for MS represent the hydrated iron oxide molecule of (Fe$_2$O$_3$.xH$_2$O) and the presence of CO group in the form of HCO$_3^-$ ion participating during corrosion, which is in agreement with findings by Renita (2015).

Conclusions

The 1-BOPAMS and 4-BOBAMS were successfully synthesized and evaluated as corrosion inhibitors of mild steel in HCl acidic medium. The inhibitors are adsorbed onto the mild steel surface by a combination of both physisorption and chemisorption (*i.e.*, mixed-type adsorption); however, chemisorption was the dominant adsorption process. Nyquist curves are represented by an imperfect semicircle loop, indicating effective inhibition of mild steel corrosion. The charge transfer resistance increased with inhibitor concentration, leading to a decrease of the corrosion rate and higher percentage inhibition efficiency. The increase of the R_P values with increasing concentration of the inhibitors indicates that the inhibition of corrosion was primarily due to protective film formation.

Conflicts of Interest

The authors declare no conflicts of interest regarding the publication of this paper.

Acknowledgements

References

ABDEL-REHIM, S.S., KHALED, K.F., and AL-MOBARAK, N.A. 2011. Corrosion inhibition of iron in hydrochloric acid using pyrazole. *Arabian Journal of Chemistry*, vol. 4, no. 3. pp. 333–337.

CHAUBEY, N., QURAISHI, M., and EBENSO, E.E. 2015. Corrosion inhibition of aluminium alloy in alkaline media by Neolamarkia cadamba bark extract as a green inhibitor. *International Journal of Electrochemistry*, vol. 10. pp. 504–518.

CHETOUANI, A., HAMMOUTI, B., AOUNITI, A., BENCHAT, N., and BENHADDA, T. 2002. New synthesised pyridazine derivatives as effective inhibitors for the corrosion of pure iron in HCl medium. *Progress in Organic Coatings*, vol. 45, no. 4. pp. 373–378.

CISSE, M.B., ZERGA, B., EL KALAI, F., TOUHAMI, M.E., SFAIRA, M., TALEB, M., HAMMOUTI, B., BENCHAT, N., EL KADIRI, S., and BENJELLOUN, A.T. 2011. Two dipodal pyridin-pyrazol derivatives as efficient inhibitors of mild steel corrosion in HCl solution - part I: Electrochemical study. *Surface Review and Letters*, vol. 18, no. 6. pp. 303–313.

EHSANI, A., NASROLLAHZADEH, M., MAHJANI, M.G., MOSHREFI, R., and MOSTAANZADEH, H. 2014a. Electrochemical and quantum chemical investigation of inhibitory of 1, 4-Ph (OX) 2 (Ts) 2 on corrosion of 1005 aluminum alloy in acidic medium. *Journal of Industrial and Engineering Chemistry*, vol. 20, no. 6. pp. 4363–4370.

EHSANI, A., MAHJANI, M.G., NASSERI, M., and JAFARIAN, M. 2014b. Influence of electrosynthesis conditions and Al$_2$O$_3$ nanoparticles on corrosion protection effect of polypyrrole films. *Anti-Corrosion Methods and Materials*, vol. 61, no. 3. pp. 146–152.

HEGAZY, M.A., AHMED, H.M., and EL-TABEI, A.S. 2011. Investigation of the inhibitive effect of p-substituted 4-(N, N, N-dimethyldodecylammonium bromide) benzylidene-benzene-2-yl-amine on corrosion of carbon steel pipelines in acidic medium. *Corrosion Science*, vol. 53, no. 2. pp. 671–678.

JACOB, K.S. and PARAMESWARAN, G. 2010. Corrosion inhibition of mild steel in hydrochloric acid solution by Schiff base furoin thiosemicarbazone. *Corrosion Science*, vol. 52, no. 1. pp. 224–228.

KIM, S., KIM, J., and MOON, I. 2011. Parameter-based model for the forecasting of pipe corrosion in refinery plants. *Industrial and Engineering Chemistry Research*, vol. 50, no. 22. pp. 12626–12629.

LOZANO, I., MAZARIO, E., OLIVARES-XOMETL, C.O., LIKHANOVA, N.V., and HERRASTI, P. 2014. Corrosion behaviour of API 5LX52 steel in HCl and H$_2$SO$_4$ media in the presence of 1, 3-dibencilimidazolio acetate and 1, 3-dibencilimidazolio dodecanoate ionic liquids as inhibitors. *Materials Chemistry and Physics*, vol. 147.s pp. 191–197.

MACDONALD, J.R. 1992. Impedance spectroscopy. *Annals of Biomedical Engineering*, vol. 20, no. 3. pp. 289–305.

MASHUGA, M.E., OLASUNKANMI, L.O., ADEKUNLE, A.S., YESUDASS, S., KABANDA, M.M., and EBENSO, E.E. 2015. Adsorption, thermodynamic and quantum chemical studies of 1-hexyl-3-methylimidazolium based ionic liquids as corrosion inhibitors for mild steel in HCl. *Materials*, vol. 8, no. 6. pp. 3607–3632.

MU, G., LI, X., QU, Q., and ZHOU, J. 2006. Molybdate and tungstate as corrosion inhibitors for cold rolling steel in hydrochloric acid solution. *Corrosion Science*, vol. 48, no. 2. pp. 445–459.

MUSA, A.Y., JALGHAM, R.T., and MOHAMAD, A.B. 2012. Molecular dynamic and quantum chemical calculations for phthalazine derivatives as corrosion inhibitors of mild steel in 1 M HCl. *Corrosion Science*, vol. 56. pp.176–183.

NATARAJA, S.E., VENKATESHA, T.V., and TANDON, H.C. 2012. Computational and experimental evaluation of the acid corrosion inhibition of steel by tacrine. *Corrosion Science*, vol. 60. pp. 214–223.

NESANE, T., MNYAKENI-MOLEELE, S.S., and MURULANA, L.C. 2020. Exploration of synthesized quaternary ammonium ionic liquids as unharmful anti-corrosives for aluminium utilizing hydrochloric acid medium. *Heliyon*, vol. 6, no. 6. pp. e04113–e04113.

RAJA, P.B., ISMAIL, M., GHOREISHIAMIRI, S., MIRZA, J., ISMAIL, M.C., KAKOOEI, S., and RAHIM, A.A. 2016. Reviews on corrosion inhibitors: a short view. *Chemical Engineering Communications*, vol. 203, no. 9. pp. 1145–1156.

RENITA, D., SANISH, T., DWIVEDI, P., and AMIT, C. 2015. Green approach to corrosion inhibition by *Emblica officinalis* (NA-7) leaves extract. *International Journal of Nano Corrosion Science and Engineering*, vol. 2, no. 3. 29–45.

THANAPACKIAM, P., RAMESHKUMAR, S., SUBRAMANIAN, S.S., and MALLAIYA, K. 2016. Electrochemical evaluation of inhibition efficiency of ciprofloxacin on the corrosion of copper in acid media. *Materials Chemistry and Physics*, vol. 174. pp. 129–137.

THIRAVIYAM, P. and KANNAN, K. 2013. Inhibition of aminocyclohexane derivative on mild steel corrosion in 1 N HCl. *Arabian Journal for Science and Engineering*, vol. 38, no. 7. pp. 1757–1767.

TOURABI, M., NOHAIR, K., TRAISNEL, M., JAMA, C., AND BENTISS, F. 2013. Electrochemical and XPS studies of the corrosion inhibition of carbon steel in hydrochloric acid pickling solutions by 3, 5-bis (2-thienylmethyl)-4-amino-1, 2, 4-triazole. *Corrosion Science*, vol. 75. pp. 123–133.

YADAV, D.K., QURAISHI, M.A., and MAITI, B. 2012. Inhibition effect of some benzylidenes on mild steel in 1 M HCl: An experimental and theoretical correlation. *Corrosion Science*, vol. 55. pp. 254–266.

ZHENG, X., ZHANG, S., GONG, M., and LI, W. 2014. Experimental and theoretical study on the corrosion inhibition of mild steel by 1-octyl-3-methylimidazolium L-prolinate in sulfuric acid solution. *Industrial and Engineering Chemistry Research*, vol. 53, no. 42. pp. 16349–16358. ◆